

*Full Length Research Paper*

## Plasma properties of nano-second laser ablated iron target in air

Muhammad Salik<sup>1</sup>, Muhammad Hanif<sup>2\*</sup>, Jiasheng Wang<sup>1</sup> and Xiqing Zhang<sup>1</sup>

<sup>1</sup>Institute of Optoelectronics, Beijing Jiaotong University, Beijing, China.

<sup>2</sup>MCS, National University of Sciences and Technology, Rawalpindi, Pakistan.

Accepted 9 September, 2013

In the present work, we studied the optical emission spectra of iron (Fe) plasma produced by the fundamental (1064 nm) and second (532 nm) wavelengths of an Nd: YAG laser. The plasma emission has been recorded spatially using five spectrometers covering the spectral region from 200 to 720 nm. The laser beam was focused on target material by placing it in air at atmospheric pressure. The experimentally observed line profiles of neutral iron (Fe I) have been used to extract the electron temperature using the Boltzmann plot method, whereas, the electron number density has been determined from the Stark broadening. The electron temperature is calculated by varying distance from the target surface along the line of propagation of plasma plume and also by varying the laser irradiance. Besides we have studied the variation of number density as a function of laser irradiance as well as its variation with distance from the target surface. It is observed that electron temperature and electron number density increases as laser irradiance is increased.

**Key words:** Iron, laser ablation, optical emission spectroscopy, electron temperature, electron number density.

### INTRODUCTION

The analytical technique employed in this study is Laser-induced breakdown spectroscopy (LIBS), which was first reported by Maker et al. (1964) and has been reviewed by several researchers (Radziemski and Cremers, 1989). This technique is based on optical detection of certain atomic and molecular species by monitoring their emission signals from the laser induced plasma, and provides a useful method to determine the chemical composition of a wide range of materials (Griem, 1997). A LIBS is a simple analytical technique as compared to many other types of elemental analysis because of its straightforward experimental set-up (Miziolek, 2006). It requires a pulsed laser for generating micro-plasma on the target surface and elemental analysis is accomplished by studying the emission of the plasma plume (Cremers and Radziemski, 2007). The laser induced plasma

characteristics depend upon several parameters, which include the features of the target, properties of the ambient medium, laser wavelength and pulse duration, etc. (Singh and Thakur, 2007). The element of iron being a good metal and have number of applications in engineering remained in focus by many researchers for long. After the invention of laser and developments in LIBS, many researchers have studied iron plasma in different aspects. Plasma plume photography and spectroscopy of Fe-oxide materials were reported by Viskup et al. (2009). Nanotechnology, nanotoxicology and neuroscience were reported by Suh et al. (2009). Stehrer et al. (2009) discussed the Laser induced breakdown spectroscopy of iron oxide powder. Two dimensional time-resolved x-ray diffraction study of dual phase rapid solidification in steels was reported by

\*Corresponding author. E-mail: drhanif-mcs@nust.edu.pk, Fax: +92-51-9270283.

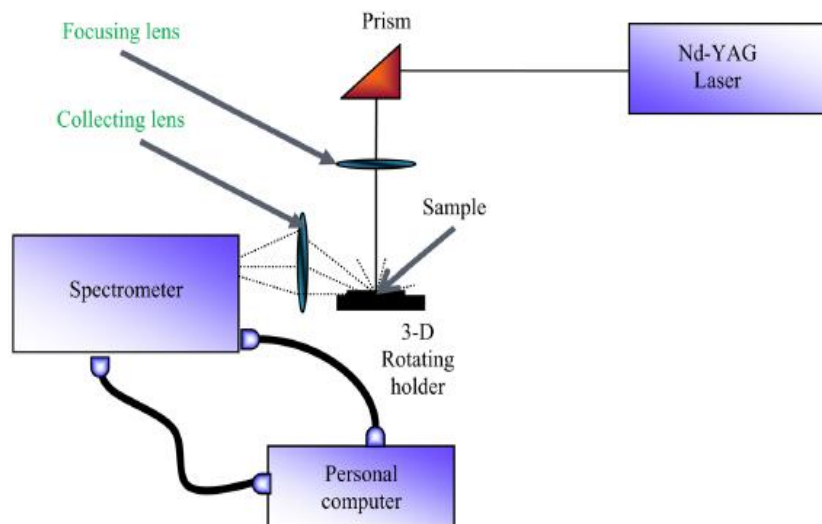


**Figure 1.** (Color online) Block diagram of the experimental setup.

Mitsuharu et al. (2010). Aswathy et al. (2010) studied an overview on iron based superconductors. Laser cladding of featureless iron-based alloy was discussed by Aghasibeig and Fredrikson (2012). Room temperature ferromagnetic multilayer thin film based on indium oxide and iron oxide for transparent spintronic applications was discussed by Gupta et al. (2010). Plasma nitriding process by direct current glow discharge at low temperature increasing the thermal diffusivity of AISI 304 stainless steel was studied by Prandel et al. (2013). Pulsed laser deposition assisted fabrication and characterization of Fe–Co nanoparticles embedded in Ti N thin film matrix was reported by Kumar et al. (2013). Gautier et al. (2013) recently studied the recent advances in theranostic nanocarriers of doxorubicin based on iron oxide and gold nanoparticles. In the present work, we have studied the spatial evolution of the iron plasma produced by the first (1064 nm) and second (532 nm) wavelengths of a pulsed Nd: YAG laser. The experimentally observed line profiles of neutral iron (Fe I) have been used to extract the electron temperature ( $T_e$ ) using the Boltzmann plot method, whereas, the electron number density ( $N_e$ ) has been determined from the Stark broadening. Beside we have studied the variation of electron temperature and electron number density as a function of laser energy at atmospheric pressure.

## EXPERIMENTAL DETAILS

The experimental setup is shown in Figure 1 and is same as that described in our previous work (Hanif et al., 2013a, b). Briefly we used a Q-switched Nd: YAG (Quantel Brilliant) pulsed laser having pulse duration of 5 ns and 10 Hz repetition rate which is capable of delivering 400 mJ at 1064 nm, and 200 mJ at 532 nm. The laser pulse energy was varied by the flash lamp Q-switch delay through the laser controller, and the pulse energy was measured by a Joule

meter (Nova - Quantel 01507). The laser beam was focused on the target using convex lens of 20 cm focal length. In the experiment, the sample studied was Iron powder containing mass percentage of 99.70% in the sample. A small amount of it was used to prepare a pallet of 15 mm diameter and 3 mm thickness with the help of hydraulic press machine using a load of 10-ton, for a time duration of 5 min. The sample was mounted on a three dimensional sample stage, which was rotated to avoid the non-uniform pitting of the target. The distance between the focusing lens and the sample was kept at 18.5 cm, less than the focal length of the lens to prevent any breakdown of the ambient air in front of the target. The spectra were obtained by averaging 10 data of single shot under identical experimental conditions. The radiation emitted by the plasma were collected by a fiber optics (high-OH, core diameter: 600  $\mu\text{m}$ ) having a collimating lens (0 - 45° field of view) placed at right angle to the direction of the laser beam. The optical fiber was connected with the LIBS - 2000 detection system (Ocean Optics Inc.), to measure the plasma emission. The emission signal was corrected by subtracting the dark signal of the detector through the LIBS software. The LIBS - 2000 detection system is equipped with five spectrometers each having slit width of 5  $\mu\text{m}$ , covering the range between 220 - 720 nm. Each spectrometer has 2048 element linear CCD array and an optical resolution of  $\approx 0.05$  nm by scanning a narrow bandwidth dye laser. In the experiments, the time delay between the laser pulses and the start of the data acquisition is about 3.5  $\mu\text{s}$ , whereas the system integration time is about 2.1 ms and stored by the OOI LIBS software. In order to record the emission spectrum, the LIBS - 2000 detection system was synchronized with the Q-switch of the Nd: YAG laser. The flash lamp out of the Nd: YAG laser triggered detection system through a four-channel digital delay/Pulse generator (SRS DG 535). The LIBS - 2000 detection system triggered the Q-switch of the Nd: YAG laser. The data acquired simultaneously by all the five spectrometers were stored on a PC through the OOILIBS software for subsequent analysis.

## RESULTS AND DISCUSSION

In the presented work, we have generated iron plasma using fundamental (1064 nm) and second (532 nm)

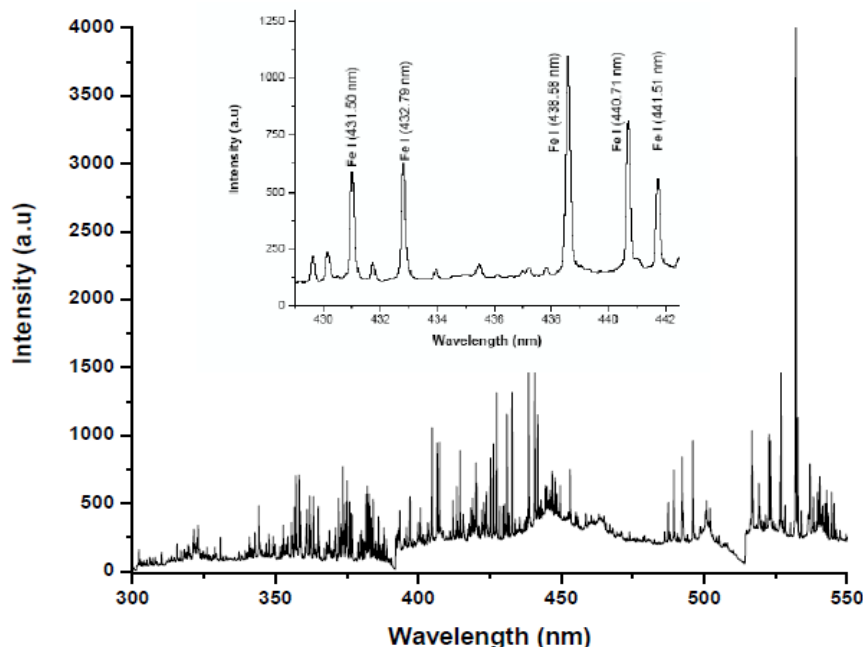


**Figure 2.** The emission spectrum of neutral iron plasma produced by the second (532 nm) wavelength of the Nd: YAG laser at a distance of 0.05 mm from the target.

**Table 1.** Spectroscopic parameters of the neutral iron lines used for the determination of plasma parameters.

S/N	Wavelength $\lambda$ (nm)	Transitions	Statistical weight		Transition probability $A_{ki}$ ( $s^{-1}$ )	Energy ( $cm^{-1}$ )	
			$g_k$	$g_i$		$E_i$	$E_k$
1	431.50	$6p6d\ ^3D_1 \rightarrow 6P^2\ ^3P_0$	5	5	$7.7 \times 10^6$	17726.981	40894.986
2	432.79	$6p7d\ ^3D_2 \rightarrow 6P^2\ ^3P_1$	5	9	$7.9 \times 10^5$	26627.604	49726.977
3	440.47	$6p7d\ ^3F_3 \rightarrow 6P^2\ ^3P_2$	7	7	$1.3 \times 10^7$	29056.321	51837.240
4	438.58	$6p7s\ ^1P_1 \rightarrow 6P^2\ ^3P_1$	9	7	$2.75 \times 10^7$	12560.930	35257.319
5	441.51	$6p7d\ ^3F_2 \rightarrow 6P^2\ ^3P_2$	7	5	$1.19 \times 10^7$	12968.549	35611.619

wavelengths of a Q-switched Nd: YAG laser. In the first set of experiments, the fundamental (1064 nm) harmonic laser having 400 mJ pulse energy, and 5 ns pulse width, was focused on the sample target placed in air at atmospheric pressure. The emission spectra of the plasma produced at the surface of the iron target is recorded at different distances along the direction of expansion of the plume. In the experimental arrangement, the laser was focused on the target surface; that is, perpendicular to the target surface, whereas, the plume emission was registered as a function of the distance parallel to the surface of the target material for the spectral region from 200 to 720 nm. Figure 2 shows the window of emission spectrum of iron plasma covering the spectral region from 300 to 550 nm, while the small window in same diagram shows the lines that we used for the determination of electron

temperature. All the observed lines in the investigated spectral region along with their assignments are listed in Table 1, based on the data by (Moore, 1971) and listed in the NBS Tables (<http://physics.nist.gov>).

After observing the well-resolved multiplet structure from a number of excited levels and decaying to a common lower level, it is tempting to extract the plasma parameters from the observed spectra; in particular, the electron number density and the plasma temperature. The electron temperature is determined using the Boltzmann plot method from the relative intensities of the observed line. The following relation has been used to extract the plasma temperature using the formula (Griem 1997):

$$\ln\left(\frac{I_{ki}\lambda_{ki}}{A_{ki}g_k}\right) = \ln\left(\frac{N(T)}{U(T)}\right) - \frac{E_k}{kT} \quad (1)$$

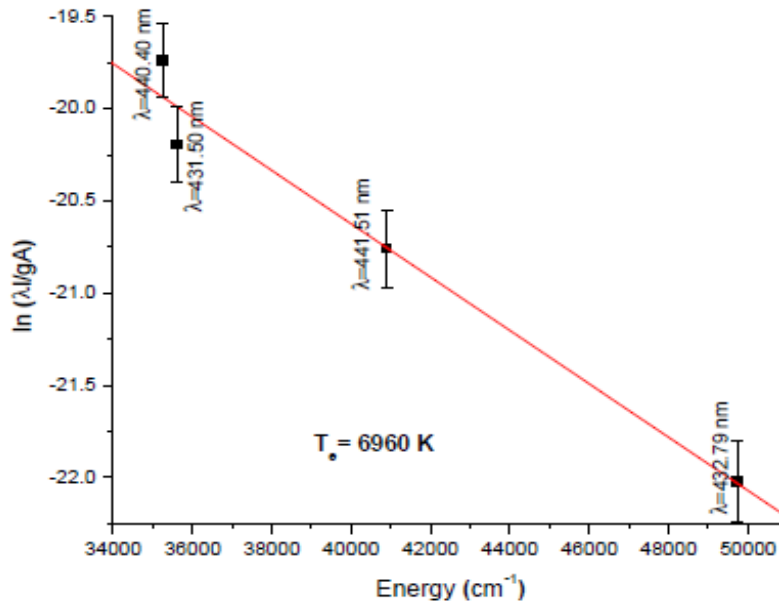


**Figure 3.** (Color online) Boltzmann plot for the neutral iron spectral lines emitted by the laser induced plasma at 0.05 mm from the target at irradiance  $4.5 \times 10^{10} \text{ W cm}^{-2}$  using the Nd: YAG laser at 532 nm.

where,  $I_{ki}$  is the integrated line intensity of the transition involving an upper level ( $k$ ) and a lower level ( $i$ ),  $\lambda_{ki}$  is the transition wavelength,  $A_{ki}$  is the transition probability,  $g_k$  is the statistical weight of level ( $k$ ),  $N(T)$  is the total number density,  $U(T)$  is the partition function,  $E_k$  is the energy of the upper level,  $k$  is the Boltzmann constant and  $T$  is the excitation temperature. A plot of  $\ln(\lambda I/gA)$  versus the term energy  $E_k$  gives a straight line with a slope equal to  $(-1/KT)$ . Thus the electron temperature can be determined without the knowledge of the total number density or the partition function. The line identifications and different spectroscopic parameters such as wavelength ( $\lambda_{ki}$ ), statistical weight ( $g_k$ ), transition probability ( $A_{ki}$ ) and term energy ( $E_k$ ) are listed in Table 1.

Four neutral iron (Fe I) lines at 431.50, 432.79, 440.47 and 441.51 nm are used for the determination of electron temperature through Boltzmann plot method. These transitions are selected as they have the greatest difference between their corresponding upper energy levels to make the Boltzmann plot more meaningful and to determine electron temperature more accurately. Errors are bound to be present in the determination of the electron temperature by this method, therefore; it is determined with  $\approx 15\%$  uncertainty, coming mainly from the transition probabilities and the measurement of the integrated intensities of the spectral lines.

Figure 3 shows the Boltzmann plot considering the data of all the observed iron lines recorded at (0.05 mm) from the surface of the plasma plume. The line which passes through the data points is a linear fit of above relation (1). The behavior of electron temperature has been studied

as function of distance from the target surface for the plasma produced by both modes of the laser. The electron temperature near the target surface is found to be higher and it varies from 7250 to 6850 K from the plasma produced by the first (1064 nm) wavelength of the laser, whereas, in case of second (532 nm) wavelength of the laser, it varies from 6980 to 6500 K over a distance range from 0.05 to 2.0 mm as shown in the Figure 4. The region near the surface of the target material constantly absorbs radiation during the time interval of the laser pulse, causing a higher temperature near the target surface.

One of the most reliable techniques to determine the electron number density is from the measured Stark broadened line profile of an isolated line of either neutral atom or singly charge ion. The electron number density ( $N_e$ ) related to the full width at half maximum (FWHM) of the Stark broadening lines is given by the relation (Griem, 1997; Cremers and Radziemski, 2007; Singh and Thakur, 2007):

$$\Delta\lambda_{1/2} = 2\omega\left(\frac{N_e}{10^{16}}\right) + 3.5A\left(\frac{N_e}{10^{16}}\right)^{1/4}\left[1 - \frac{3}{4}N_D^{-1/3}\right]\omega\left(\frac{N_e}{10^{16}}\right) \quad (2)$$

Where,  $\omega$  is the electron impact width parameter,  $A$  is the ion broadening parameter,  $N_e$  is the electron number density and  $N_D$  is the number of particles in the Debye sphere. The first term in Equation 2 refers to the broadening due to the electron contribution, whereas, the second term is attributed to the ion broadening. Since the contribution of the ionic broadening is normally very

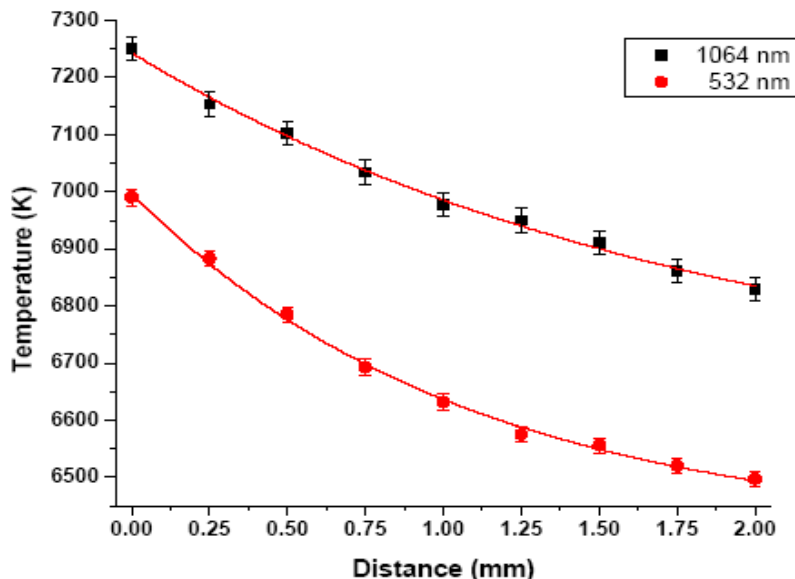


**Figure 4.** (Color online) variation of the electron temperature along the direction of propagation of the plasma plume using fundamental (1064 nm) and second (532 nm) wavelengths of Nd: YAG laser.

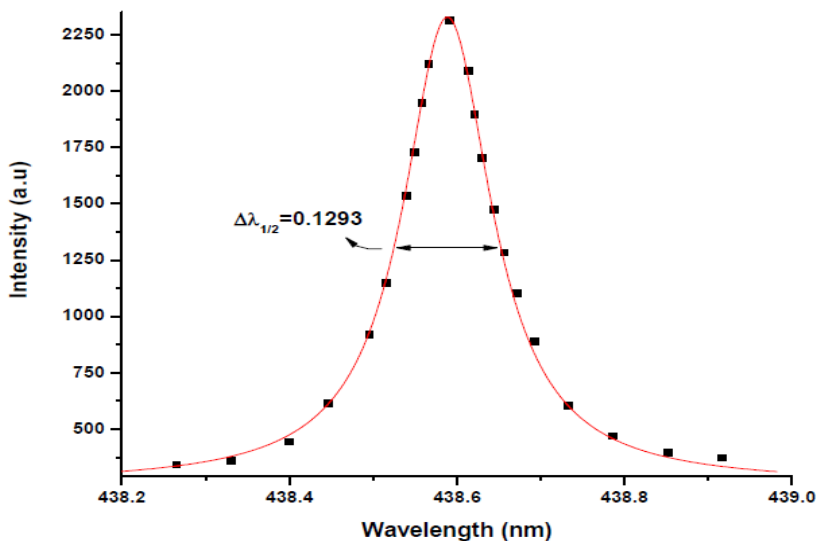


**Figure 5.** (Color online) Stark broadening profile of neutral iron line at 438.58 nm. The dots represent the experimental profile and the solid line is Lorentzian fit at a distance of 0.05 mm from the target.

small, therefore, it can be neglected and Equation 2 reduced to:

$$\Delta\lambda_{1/2} = 2\omega \left( \frac{N_e}{10^{16}} \right) \tag{3}$$

Here  $\Delta\lambda_{1/2}$  is the width of the spectral line,  $\omega$  is the electron impact broadening parameter and  $N_e$  is the electron number density. The value of  $\omega$  corresponding to

different electron temperatures is obtained from the reference data (Griem, 1997). The electron number densities have been determined from the line profiles of the isolated iron neutral lines at 538.34 nm using Relation 3 and  $\Delta\lambda_{1/2}$  is extracted by fitting the Lorentzian line shape to the observed data.

Figure 5 shows the line profile of the neutral iron line at 438.50 nm recorded from the plasma, along with the least squares fit of a Lorentzian line shape which yields the width  $\Delta\lambda_{1/2}$  of this line. The condition that the atomic

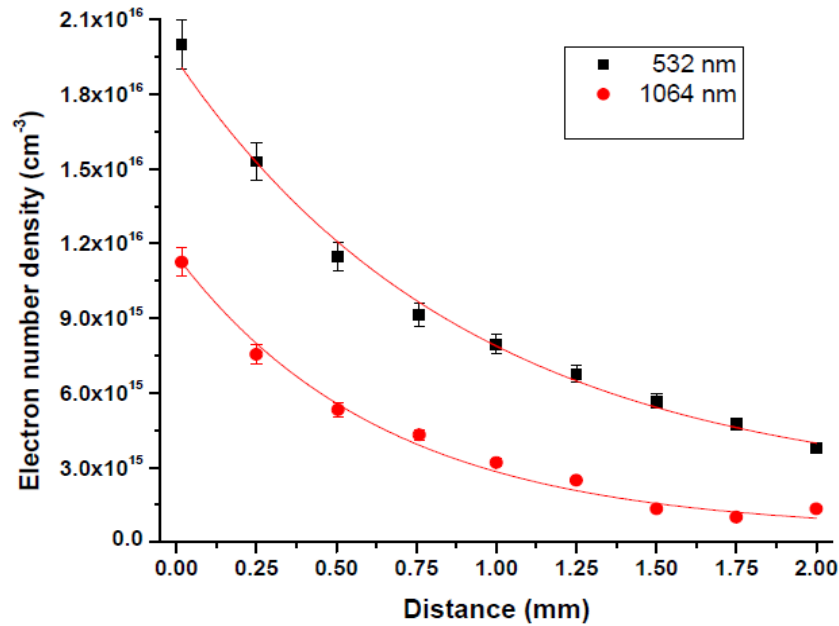


**Figure 6.** (Color online) Variation of the electron number density with the distance using the fundamental (1064 nm) and second (532 nm) wavelengths of Nd: YAG laser.

states should be populated and depopulated predominantly by electron collisions, rather than by radiation, requires an electron density which is sufficient to ensure the high collision rate. The corresponding lower limit of the electron density is given by the Mc Whirter criterion (Mc Whirter, 1965) to check the condition for the validity of the local thermodynamic equilibrium (LTE):

$$N_e \geq 1.6 \times 10^{12} T^{1/2} (\Delta E)^3 \quad (4)$$

Here  $T$  (K) is the plasma temperature and  $\Delta E$  (eV) is the energy difference between the states, which are expected to be in LTE. At  $\sim 7000$  K, Equation 4 yields  $N_e \approx 1.6 \times 10^{14} \text{ cm}^{-3}$ . The electron number densities determined in our experiments are higher than the required number density which satisfies the LTE condition. Figure 6 shows the number densities for both wavelengths of the laser. The values of number densities using fundamental and second harmonic of the Nd: YAG laser with laser irradiance  $6.5 \times 10^{10} \text{ W cm}^{-2}$  are determined as  $1.12 \times 10^{16}$  and  $2 \times 10^{16} \text{ cm}^{-3}$  respectively. These values decrease to  $1.38 \times 10^{15}$  and  $3.75 \times 10^{15} \text{ cm}^{-3}$  over distance ranges from 0.05 to 2.0 mm from the target surface respectively for neutral iron line at 538.34 nm. The decrease in the number density at large distance is mainly due to the recombination of electrons and ions. As is evident from the Figures 4 and 6, the electron temperature and the electron number density both close to the target are maxima, since the region close to the

surface continuously absorbs the laser radiation during the laser pulse. When the plasma expands, it thermalizes by transferring the energy to its surroundings and is transparent to the laser pulse; therefore, both plasma parameters decrease along the direction of expansion of the plume. Moreover, the electron temperature and number density decrease rapidly within a short distance from the target surface, while at a large distance, they exhibit little variation. The variation in the electron temperature is slower as compared to that of number density. The internal energy of the plasma is distributed in its thermal and ionization energy. The particle density in the plasma depends on the degree of ionization, evaporation rate and the plasma expansion velocity. Because of the high expansion velocity of the leading plasma edge, the electron density decreases, makes the plasma transparent to the laser beam at larger distance away from the target surface. The absorption in the plasma mainly occurs by an inverse bremsstrahlung and photo ionization process.

In the second set of experiments, we have determined the electron temperature and electron number density for different values of the fundamental (1064 nm) and second (532 nm) wavelengths of Nd: YAG laser. It is observed that the intensities and widths of the spectral lines increase with the increase in the laser irradiance. Figure 7 shows the variation of the electron temperature for the fundamental (1064 nm) and second (532 nm) wavelengths of the laser produced plasma with respect to the laser irradiance at which the temperature varies

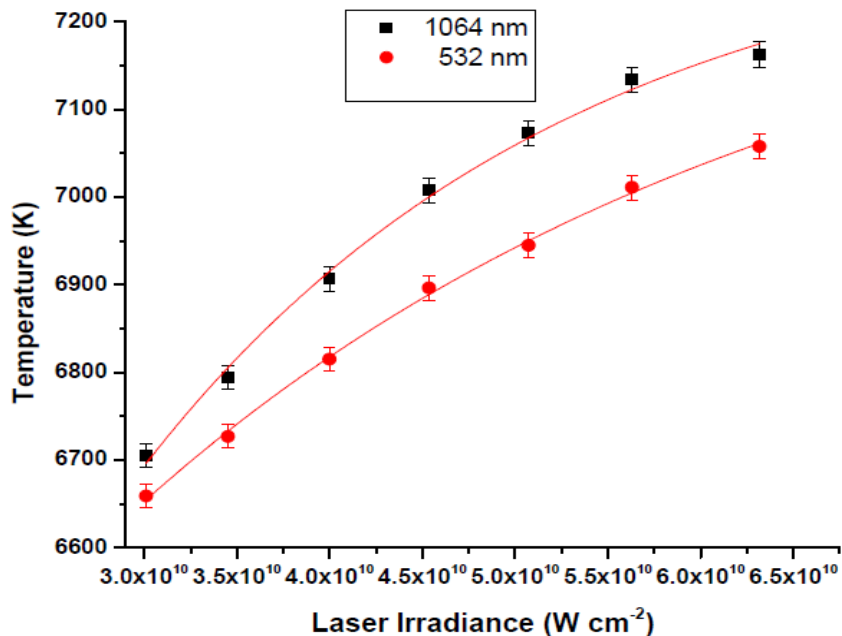


**Figure 7.** (Color online) Variation of the electron temperature with the laser irradiance using second (532 nm) wavelength of Nd: YAG laser at a distance of 0.05 mm from the target.

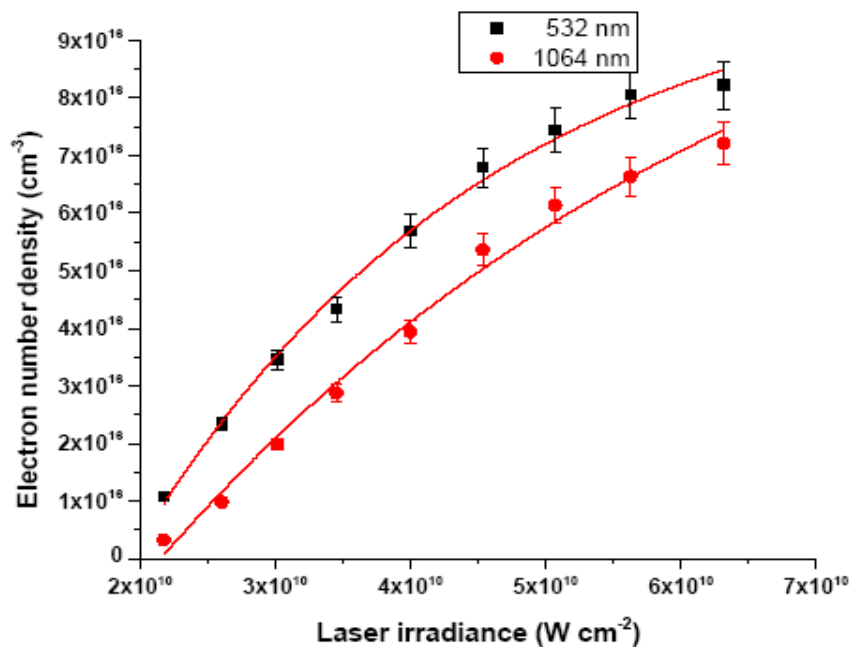


**Figure 8.** (Color online) Variation of the electron number density with the laser irradiance using first (1064 nm) wavelength of Nd: YAG laser at a distance of 0.05 mm from the target.

from 7165 to 6705 K and from 7060 to 6660 K at a distance of 0.05 mm from the target surface respectively. Evidently, the electron temperature increases with the

increase in the laser irradiance. Figure 8 shows the variation in the electron number density as a function of the laser irradiance in case of fundamental (1064 nm)

and second (532 nm) wavelengths of the laser. The variation in the electron number density with the laser irradiance also shows a similar behaviour. The irradiance varies from  $6.50 \times 10^{10}$  to  $7.25 \times 10^{10}$  watt  $\text{cm}^{-2}$ , whereas electron number densities vary from  $3.29 \times 10^{15}$  to  $7.22 \times 10^{16}$   $\text{cm}^{-3}$  and  $1.08 \times 10^{15}$  to  $8.22 \times 10^{16}$   $\text{cm}^{-3}$  for fundamental (1064 nm) and second (532 nm) wavelengths of the laser respectively. The increase in the plasma temperatures and electron number densities vary slowly, this may be attributed to the plasma shielding. The observed increase in plasma parameters ( $N_e$  and  $T_e$ ) by the increase of the laser energy is due to the absorption and/or reflection of the laser photon by the plasma, which depends upon the plasma frequency. In our experiment, the corresponding frequency is  $2.8 \times 10^{14}$  Hz, whereas the plasma frequency is  $\nu_p = 8.9 \times 10^3 \sqrt{N_e}$ . The electron number density is  $N_e \approx 10^{15}$   $\text{cm}^{-3}$ , therefore,  $\nu_p = 3.6 \times 10^{12}$  Hz which is less than the laser frequency ( $\approx 10^{14}$  Hz), which shows that the energy loss due to the reflection of the laser radiation from the plasma is insignificant.

## Conclusion

The LIBS method has been successfully applied as an analytical technique for the analysis of iron plasma using the fundamental (1064 nm) and second (532 nm) harmonics of an Nd: YAG laser. We have determined the electron temperature and the electron number density along the axial position of the plume. It is observed that the spatial behaviour of the electron temperature close to the target is maximum and decreases along the distance from the target, whereas the electron number density close to the target is maximum and decreases as  $1/d$ . Variations of the electron temperature and the electron number density with the laser irradiance shows that both these parameters increase with the increase of the laser irradiance. The values of the plasma parameters ( $N_e$  and  $T_e$ ) determined are well within the range as reported in the previous literature.

## REFERENCES

- Aswathy PM, Anooja JB, Sarun PM, Syamaprasad U (2010). Topical Review: An overview on iron based superconductors. *SuperconD. Sci. Tech.* 23:073001-073020.
- Aghasibeig M, Fredriksson H (2012). Laser cladding of a featureless iron-based alloy. *Surf. Coat. Tech.* 209:32-37.
- Cremers DA, Radziemski LJ (2007). *Handbook of Laser-Induced Breakdown Spectroscopy*: New York: Wiley.
- Gautier J, Allard-Vannier E, Munnier E, Souce M, Chourpa I (2013). Recent advances in theranostic nanocarriers of doxorubicin based on iron oxide and gold nanoparticles. *J. Controlled Release* 169:48–61.
- Griem HR (1997). *Principles of Plasma Spectroscopy*: Cambridge University Press. 10.1017/CBO9780511524578.
- Gupta RK, Ghosh K, Kahol PK (2010). Room temperature ferromagnetic multilayer thin film based on indium oxide and iron oxide for transparent spintronic applications. *Mater. Lett.* 64:2022–2024.
- Hanif M, Salik M, Baig MA (2013a). Optical spectroscopic studies of titanium plasma produced by an Nd: YAG Laser. *Opt. Spectrom.* 114:7-14.
- Hanif M, Salik M, Sheikh MN, Baig MA (2013b). Laser-based optical emission studies of barium plasma. *Appl. Phys. B: Lasers Optics* 110:563-571.
- Kumar D, Sarin A, Verma V, Venkatraman R (2013). Pulsed laser deposition fabrication and characterization of Fe–Co nanoparticles embedded in TiN thin film matrix. *Thin Solid Films* 534:561–565.
- Maker PD, Terhune RW, Savage CM (1964). *Quantitative Electronics*, Proceedings of the 3<sup>rd</sup> International Conference: Columbia University Press, New York.
- Mc Whirter RWP (1965). *Plasma diagnostic techniques*. New York: Academic Press.
- Mitsuharu Y, Takahiro O, Hidenori T, Yuichi K, Masugu S, Hidenori, Akiko N (2010). Two-dimensional time-resolved x-ray diffraction study of dual phase rapid solidification in steels. *J. Appl. Phys.* 107: 013523-013523-6.
- Moore CE (1971). *Atomic Energy Levels*, NBS circular No. 467, Washington DC.
- Miziolek AW, Palleschi V, Schechter I (2006). *Laser-induced breakdown spectroscopy (LIBS): Fundamentals and applications*. Cambridge University Press.
- Prandel L, Somer V, Assmann A, Camelotti A, Costa F, Bonardi G, Jurelo C, Rodrigues AR, Cruz GK (2013). Plasma nitriding process by direct current glow discharge at low temperature increasing the thermal diffusivity of AISI 304 stainless steel. *J. Appl. Phys.* 113: 063507-063507-5.
- Radziemski LJ, Cremers DA (1989). *Laser-induced plasma and applications*. New York.
- Singh JP, Thakur SN (2007). *Fundamental of Laser-Induced Breakdown Spectroscopy*: Elsevier B.V.
- Stehrer T, Praher B, Viskup R, Jasik J, Wolfmeir H, Arenholz E, Heitz J, Pedarnig JD (2009). Laser-induced breakdown spectroscopy of iron oxide powder. *J. Anal. At. Spectrom.* 24:973-978.
- Suh WH, Stucky GD, Suh YH (2009). Nanotechnology, nanotoxicology and neuroscience. *Progress Neurobiol.* 87:133-170.
- Viskup R, Praher B, Stehrer T, Jasik J, Wolfmeir H, Arenholz E, Pedarnig JD, Heitz J (2009). Plasma plume photography and spectroscopy of Fe-oxide materials. *Appl. Surf. Sci.* 255:5215-5219.